# Trustworthy Analysis of Recent Debris Cloud Conjunction Events Using an Adaptive Monte Carlo Forecasting Platform

Undergraduate Thesis

Presented in Partial Fulfillment of the Requirements for
Graduation with Research Distinction in the
Department of Mechanical and Aerospace Engineering at
The Ohio State University

by

**Alexandra Mangel**

April 2022

Advisor: Dr. Mrinal Kumar

**Abstract**

Every untracked, inactive, or unfamiliar object in Earth's orbit poses a risk to satellites and rockets that wish to safely navigate through space. Objects of this nature, known as "space debris," will remain in orbit without deliberate intervention. The purpose of this project is to perform a highly accurate retrospective analysis of a certain outstanding close-approach event (also known as a conjunction event) that occurred in the geostationary belt. It is expected that the successful completion of this work will result in a trustworthy prognostics tool that can help minimize, or even eliminate, such risk in the future. Events related to candidate resident space objects were considered, and the 2016 Briz-M rocket body explosion was chosen as the particular event of interest. By appropriately modeling the motion of such candidates through astrodynamics analysis and adjusting the initial conditions to reflect sensor precision, a recently developed adaptive Monte Carlo method, a MATLAB-based forecasting platform, can be employed to propagate a particle cloud representing the object's orbit over time. The completion of this project will validate the methods used, while simultaneously reducing the risks of collision and damage in similar events in the future.

**Acknowledgements**

The completion of this thesis would not be possible without contributions from my advisor, Dr. Mrinal Kumar. I would like to extend my gratitude to him for enabling me to join the Laboratory for Autonomy in Data-Driven and Complex Systems, and providing me the space and guidance to work on this project. Dr. Kumar has encouraged me to think critically on a much deeper level, and his support has allowed me to feel confident pursuing graduate studies. I also want to thank him for giving me the opportunity to co-author and present my first published work at SciTech, an amazing international AIAA conference. I would also like to extend my gratitude to Ph.D. student, and my co-author, Andrew VanFossen. Without his patience I would have not been able to conquer adaptive Monte Carlo.

I would like to give a special thank you to Dr. Jim Gregory. His time as my professor at Ohio State not only inspired me to pursue undergraduate research, but kickstarted this whole journey, leading up to a graduating with a research distinction. Likewise, I want to thank Dr. Matt McCrink for being my first advisor and seeing my potential as a research scientist.

Thank you to the Ohio Space Grant Consortium for sponsoring this work and featuring it in their 2021-2022 Student Research Symposium Proceedings.

Finally, I would like to thank my family and friends for being my backbone, for providing me with so much love and support, for being patient with me, and for all the times you listened to me talk about this work. It means the world to me.

## Table of Contents

**List of Figures**

**List of Tables**

## I. Introduction

### Section 1: Orbital Debris

With each passing year, the skies above Earth are increasingly filled with incredible feats of technology, blinking as they provide valuable data back to the humans who put them there. Ansys: Government Initiatives (AGI) predicts that by 2027, there will be over 30,000 man-made objects in Earth's orbit [1]. For the first 50 years of the space age, dozens of new satellites were launched every year, but since the turn of the century, that number has grown by hundreds, culminating in the launch of over 1,400 satellites in 2021 alone [2]. However, as the number of satellites in orbit continues to grow, so does the quantity of defunct satellites. Regardless of whether an orbiter lost connection, broke, or its mission simply came to an end, objects that can no longer be monitored will remain in orbit without purposeful intervention and are colloquially known as "space debris." The presence of these inactive satellites poses a significant risk of conjunction, or collision, to operating bodies in Earth's orbit, such as active autonomous satellites and rockets passing through to outer space. A commonly referenced example of this risk is the 2009 collision between two communications satellites; the then-operational American Iridium 33 and the already decommissioned Russian Cosmos 2251. This was the first occurrence of a conjunction event between two intact spacecraft moving at a high velocity in low Earth orbit (LEO) [3]. Just after the collision, the U.S. Space Surveillance Network (SSN) found over 700 new pieces of debris spread across LEO and even predicted that this number could have been larger if the two bodies made contact head-on. Since then, the number of objects being tracked from this event has grown to over 2,300, and are expected to remain in orbit for decades, posing a large hazard to other satellites in LEO. The operating altitude of Iridium contains approximately 3,300 other objects and close approaches are common between them. Near the end of 2021, the International Space Station had to make two maneuvers in the same orbit regime to move out of the way of debris expected to make a close approach of merely a few kilometers [4].

More than 27,000 objects are currently being tracked by the SSN, but the quantity of orbital debris continues to grow as smaller objects are accounted for. Objects the size of a softball might not initially seem like a risk to a spacecraft, but these pieces of junk are moving at 17,500 miles per hour [5]. Such a large quantity of debris begets the need for accurate forecasting to predict conjunction events so that they can be prevented, like the aforementioned case with the ISS, which has had to make dozens of such maneuvers in its lifetime. It is infeasible to continuously monitor all tens of thousands of these resident space objects (RSOs) to ensure a particular orbiting body has a safe path forward for its operational lifetime. This is why predictive analysis becomes so important; being able to ascertain the path of a piece of debris at the same altitude as your active orbiting body can determine the likelihood of the two RSOs making a close approach, and thus provide an estimate of probability of collision. If conjunction risk is determined to be high enough, appropriate adjustments to the active orbiter can be made and the chances of collision drastically reduced.

**Section 2: Space Situational Awareness**

Space Situational Awareness (SSA) is the intersection between analysis within the space domain and surveillance of satellites and their surrounding environment [6]. SSA includes methods used to guide autonomous systems through potentially hazardous environments by determining the likelihood of risk, particularly of collision with other objects. SSA can be used in any environment but is of particular use in geosynchronous Earth orbit (GEO) because of the high density of objects. GEO has seen a recent increase in the number of RSOs, particularly at the geostationary level, because a satellite at this altitude will rotate with Earth, making one complete orbit each day with minimal chance of perturbations from this state. Commercial satellites operating at the geostationary level are further required to maintain longitude within a very tight range, i.e., ±0.05° to ±0.1°. In order to monitor such satellites to ensure they adhere to this requirement, a need for more robust forecasting and propagation models arose, eventually leading to the development of the adaptive version of the Monte Carlo platform discussed in this paper.

The Monte Carlo method has been used for a variety of purposes to model dynamical systems because of its provable asymptotic convergence and parallelizability. The Monte Carlo platform is a collection of MATLAB algorithms that use ensemble-based simulations to create a cloud of particles to probabilistically represent the state of an object of interest and the uncertainty in its predicted path over time. Monte Carlo produces an evolved state-uncertainty for the object by taking a randomized distribution of particles from the underlying probability space and propagating each particle forward using the system dynamics, resulting in a new ensemble representing the object's state after a defined amount of time. A problem arises with Monte Carlo in that it cannot hold its level of accuracy when evolving the new state-space if it keeps the number of particles constant. Thus, an "adaptive" version of this platform was developed to create a closed-loop architecture so that particles can be added or removed to maintain robustness in accuracy and computing time. The performance of the adaptive Monte Carlo (AMC) platform is measured using a "quantity of interest" (QoI), which changes depending on the application. The user will prescribe an upper bound for estimation error, and if the QoI exceeds this, the AMC algorithm will determine the next ideal particle to add to the ensemble, to be propagated from $t_0$ all the way to the current state $t$. Likewise, the QoI is restricted by the user-prescribed lower bound. If the QoI is lower than this, AMC activates a particle removal scheme proportional to the particle's current state-probability density function (pdf) to "halt" the propagation of that particle in order to reduce computational load. The inclusion of these particle addition and removal algorithms enables AMC to represent the state uncertainty with a minimized ensemble size, which dramatically saves computation time without losing the guaranteed prescribed bounds of accuracy [7]. Due to the fact that the platform produces simulation results at a level of precision defined by the user, AMC is defined as being able to create *trustworthy* SSA by successfully capturing the motion of objects in orbit with this controlled level of accuracy [8].

**Section 3: The Briz-M Explosion and Quantity of Interest**

The focus of this paper is an analysis of a particular event of interest in GEO, namely the Briz-M rocket body breakup (also stylized as *Breeze-M*). In January 2016, Briz-M (2015-075B), the upper rocket stage designed for injecting payloads into GEO, suddenly exploded, only a month after launching the Cosmos 2513 Russian military satellite [9]. The rocket stage fragmented into several pieces, generally falling within a 0.23-0.56 meter range in size [10], and the North American Aerospace Defense Command (NORAD) was able to determine position and velocity data just after conjunction for the a portion of those fragments [11]. The purpose of this research is to get an assessment of the probability of collision of these fragments with each other. The strategy is to utilize the AMC platform, coupled with an appropriate quantity of interest, to propagate the orbits of the Briz-M fragments to determine their closest approach in space.

As stated earlier, choosing a QoI is essential to getting a precise evaluation of the AMC performance. The error associated with estimating the QoI is what drives the particle addition and removal platforms. If $\mathbf{x}_t$ represents the current state with a pdf $\mathcal{W}_t(\mathbf{x}_t) \equiv \mathcal{W}_t$, and $h(\mathbf{x}_t)$ is a function of the state, then the QoI is the expected value of a function of the state, $\bar{h}(\mathbf{x}_t)$ [8]. Generally, QoIs are defined as shown in Equation 1:

$$\bar{h}(\mathbf{x}_t) \triangleq E_{\mathcal{W}_t}[h(\mathbf{x}_t)] = \int_{\Omega_t} h(\mathbf{x}_t)\mathcal{W}_t d\mathbf{x}_t \tag{1}$$

where $E_{\mathcal{W}_t}$ is the expected value operator and $\Omega_t$ is the state-space at time $t$. Selection and definition of the application-specific QoI for this research will be detailed in the methodology section of this paper.

The significance of this project is the completion of a robust and precise orbital forecasting of the Briz-M rocket body and its largest pieces of debris. By being able to predict the path of these objects, future conjunction events can be avoided, and the risk of creating more debris minimized. Additionally, each iteration of the AMC platform further validates the Monte Carlo method and ensemble enhancement algorithm.

The rest of this thesis is outlined as follows. The following section will detail the methodology of the research, including developing the uncertainty propagation platform and defining quantity of interest. Next is the results section, starting with development of the dynamical model of the system, then iterating the AMC platform and an analysis of the risk of conjunction. Finally, conclusions concerning this event will be made and well as a discussion of future work.

## II. Methodology

### Section 1: Uncertainty Propagation with Monte Carlo

Broadly, the goal of Monte Carlo is to determine a solution to a nonlinear continuous dynamic system with some initial condition uncertainty. The platform is modeled by the stochastic differential equation, shown in Equation 2 [12]:

$$d\mathbf{x} = \mathbf{f}(t, \mathbf{x})dt \quad , \quad \mathbf{x}_0 \sim \mathcal{W}_0(t_0, \mathbf{x}) \tag{2}$$

where $\mathbf{x}$ describes the system state and $\mathbf{x}_0$ is the initial condition with probability density function $\mathcal{W}_0$. A pdf shows the relative likelihood that the value of a random variable would be close to a sample within a sample space. The time evolution of the state-pdf $\mathcal{W}_0(t_0, \mathbf{x})$ is given by the stochastic Liouville equation:

$$\frac{\partial}{\partial t}\mathcal{W}(t, \mathbf{x}) = \mathcal{L}[\mathcal{W}(t, \mathbf{x})] = -\sum_{i=1}^{N}\left( f_i \frac{\partial \mathcal{W}}{\partial x_i} + \mathcal{W}\frac{\partial f_i}{\partial x_i}\right) \tag{3}$$

where $\mathcal{L}[\cdot]$ is the stochastic Liouville operator and estimates the uncertainty of the propagated state. The relative motion of the RSOs in GEO are described by $\mathbf{f}(t, \mathbf{x})$ and their Keplerian motion with small orbital perturbations are represented by the classical two-body problem:

$$\mathbf{r} = -\frac{\mu_\oplus}{\|\mathbf{r}\|^3}\mathbf{r} + \mathbf{F}(\mathbf{r}) \tag{4}$$

It is pertinent that the orbital elements are represented in the equinoctial coordinate frame, and the purpose of this is to avoid nonlinearities that would otherwise be present with traditional Cartesian

coordinates [8]. The traditional Cartesian elements, instantaneous Keplerian orbital elements, and equinoctial elements are shown below, respectively.

$$\mathbf{x}_{CE} = \begin{bmatrix} x \\ y \\ z \\ v_x \\ v_y \\ v_z \end{bmatrix}, \ \mathbf{x}_{OE} = \begin{bmatrix} a\text{: semi} - \text{major axis} \\ e\text{: eccentricity} \\ i\text{: inclination} \\ \Omega\text{: ascending node} \\ \omega\text{: argument of perigee} \\ M\text{: mean anomaly} \end{bmatrix}, \ \mathbf{x}_{EE} = \begin{bmatrix} a \\ P_1 = e\sin\varpi \\ P_2 = e\cos\varpi \\ Q_1 = \tan\frac{1}{2}i\sin\Omega \\ Q_2 = \tan\frac{1}{2}i\cos\Omega \\ l = \varpi + M \end{bmatrix} \tag{5}$$

The variables $(P_1, P_2)$ and $(Q_1, Q_2)$ correspond to the eccentricity and inclination vectors, respectively, where $\varpi = \Omega + \omega$ and $l$ is the mean equinoctial anomaly. The governing equations of motion of an RSO in GEO with perturbations take the following form in the equinoctial coordinate system:

$$\frac{da}{dt} = \frac{2a^2}{h}\left[(P_2\sin L - P_1\cos L)a_{dr} + \frac{p}{r}a_{d\theta}\right] \tag{6a}$$

$$\frac{dP_1}{dt} = \frac{r}{h}\{-\frac{p}{r}\cos L a_{dr} + \left[P_1 + \left(1+\frac{p}{r}\right)\sin L\right]a_{d\theta} - P_2(Q_1\cos L - Q_2\sin L)a_{dh}\} \tag{6b}$$

$$\frac{dP_2}{dt} = \frac{r}{h}\{\frac{p}{r}\sin L a_{dr} + \left[P_2 + \left(1+\frac{p}{r}\right)\cos L\right]a_{d\theta} + P_1(Q_1\cos L - Q_2\sin L)a_{dh}\} \tag{6c}$$

$$\frac{dQ_1}{dt} = \frac{r}{2h}(1+Q_1^2+Q_2^2)\sin L a_{dh} \tag{6d}$$

$$\frac{dQ_2}{dt} = \frac{r}{2h}(1+Q_1^2+Q_2^2)\cos L a_{dh} \tag{6e}$$

$$\frac{dl}{dt} = n - \frac{r}{h}\left\{\begin{matrix}\left[\frac{a}{a+b}\left(\frac{p}{r}\right)(P_1\sin L + P_2\cos L) + \frac{2b}{a}\right]a_{dr} \\ +\frac{a}{a+b}\left(1+\frac{p}{r}\right)(P_1\cos L - P_2\sin L)a_{d\theta} + (Q_1\cos L - Q_2\sin L)a_{dh}\end{matrix}\right\} \tag{6f}$$

where

$$b = a\sqrt{1-P_1^2-P_2^2} \qquad h = nab$$

$$\frac{p}{r} = 1 + P_1\sin L + P_2\cos L \qquad \frac{p}{r} = \frac{h}{\mu_\oplus(1+P_1\sin L + P_2\cos L)}$$

and $L = \varpi + f$ is the true equinoctial anomaly (where $f$ is the true anomaly), and can be obtained by first solving the Keplerian equation

$$l = K + P_1 \cos K - P_2 \sin K \tag{7}$$

for the eccentric equinoctial anomaly $K$ (eccentric longitude). The distance between the RSO and Earth $r$ can be determined via

$$r = a(1 - P_1 \sin K - P_2 \cos K). \tag{8}$$

Following this, $L$ can be calculated from these relationships:

$$\sin L = \frac{a}{r}\left[\left(1 - \frac{a}{a+b}P_2^2\right)\sin K + \frac{a}{a+b}P_1 P_2 \cos K - P_1\right] \tag{9a}$$

$$\cos L = \frac{a}{r}\left[\left(1 - \frac{a}{a+b}P_1^2\right)\cos K + \frac{a}{a+b}P_1 P_2 \sin K - P_2\right] \tag{9b}$$

where

$$\frac{a}{a+b} = \frac{1}{1+\sqrt{1-P_1^2-P_2^2}}\ . \tag{10}$$

Since the shape of the Earth is not an exact sphere, the disturbance acceleration terms $\mathbf{a}_d = [a_{dr}, a_{d\theta}, a_{dh}]$ are given as:

$$\mathbf{a}_d = \frac{\mu_\oplus}{r^2}\sum_{k=2}^{4} J_{k,E}\left(\frac{r_E}{r}\right)^k [P'_{k+1}\mathbf{i}_{SO} - P'_k \mathbf{i}_z] \tag{11}$$

where

$$P'_2 = 3\cos\phi \qquad P'_4 = \frac{1}{3}(7\cos\phi P'_3 - 4P'_2)$$

$$P'_3 = \frac{1}{2}(5\cos\phi P'_2 - 3) \qquad P'_5 = \frac{1}{4}(9\cos\phi P'_4 - 5P'_3)$$

are the derivatives of the Legendre polynomials [13] and $\cos\phi = \mathbf{i}_{SO} \cdot \mathbf{i}_z$ the cosine of the angle $\phi$ between the unit vector $\mathbf{i}_{SO}$ pointing towards the RSO from the center of the Earth and the unit vector $\mathbf{i}_z$ point towards the north pole. The variable $r_E$ = 6378.137 km is the equatorial radius of the Earth and $J_{2,E}$ = 0.00108263, $J_{3,E} = -0.00000254$, and $J_{4,E} = -0.00000161$ are the coefficients of the second, third, and fourth harmonics of Earth's potential function, respectively [14]. Considering that solar radiation pressure is several orders of magnitude less than $J_2$ and atmospheric drag is essentially zero in GEO [5], the only disturbing forces accounted for in this problem setup are the $J_2$ effect ($10^{-5}$) and the additional forces resulting from Earth's non-spherical nature ($10^{-7}$).

**Section 2: Adaptive Monte Carlo**

The Monte Carlo suite of algorithms functions by creating a cloud of particles based on the initial state of the system, and then each particle is propagated forward in time using the system dynamics. Refer again to Equation 2:

$$d\mathbf{x} = \mathbf{f}(t, \mathbf{x})dt \quad , \quad \mathbf{x}_0 \sim \mathcal{W}_0(t_0, \mathbf{x}) \tag{2}$$

Monte Carlo discretizes the initial state pdf by creating an ensemble cloud of particles, $\{x_0^i\}_{i=1}^n \sim \mathcal{W}_0$, and each particle is propagated forward in time using the system dynamics. This creates an evolved state pdf after some amount of time, $\{\Phi_t\ (x_0^i)\}_{i=1}^n \approx \mathcal{W}_t$, where $\Phi_t$ maps the system dynamics via: $\mathbf{x}_t^i = \Phi_t(\mathbf{x}_0^i)$. The particle cloud represents the system's uncertainty. The challenge with this setup is deciding the value of $n$, the number of particles in the ensemble. The cloud must have enough particles to ensure the propagation is trustworthy, but not so many particles that it becomes too computationally intensive. This is where Monte Carlo becomes "adaptive", so that $n$ can be optimized. Thus, it is essential to determine precise performance metrics and define accuracy bounds, as well as measure those metrics iteratively, in order to adjust the Monte Carlo ensemble with each iteration to meet those defined accuracy bounds.

Choosing an appropriate quantity of interest is essential to getting a precise evaluation of the AMC performance. The error associated with estimating the QoI is what drives the particle addition and

removal platforms. If QoI is defined as $\bar{h}$, referring to Equation 1, then $\tilde{h}_n$ is the Monte Carlo estimate of the QoI. The Monte Carlo estimation error is the difference between these two values, denoted by epsilon:

$$|\varepsilon_n| = \left|\bar{h} - \tilde{h}_n\right| \tag{12}$$

The estimation error is upper bounded by the product of the discrepancy of the ensemble and the variation of the system dynamics:

$$|\varepsilon_n| = \left|\bar{h} - \tilde{h}_n\right| \leq \mathcal{D}(\{x_0^i\}_{i=1}^n)V(S_t) \tag{13}$$

The change is system dynamics, $V(S_t)$, is not controllable, so the discrepancy of the ensemble, $\mathcal{D}(\{x_0^i\}_{i=1}^n)$, is controlled with a user-defined limit. When the ensemble's accuracy is above this user-defined upper bound, the ensemble enhancement routine is activated, minimizing the discrepancy cost function to find the next optimal particle. The new AMC ensemble will be identical to the old one at $t_0$, with the addition of the newly added particle, which is propagated from $t_0$ to the current time. It is noted here that a particle removal scheme was not used for this problem. Thus, the final step in the problem setup is to define $\bar{h}$, the QoI.

**Section 3: Defining Quantity of Interest**

While the most obvious choice for QoI is probability of collision, modeling this becomes way too computationally intensive for the AMC platform [15]. For the geostationary Briz-M event, the trace of the position covariance matrix was selected as the QoI.

To understand this value, start with the *expectation*, or mean value of a discrete random variable X with pmf $f_{\mathrm{X}}(\cdot)$, defined as:

$$\mathrm{E}[g(\mathrm{X})] = \sum_x g(x) f_{\mathrm{X}}(x) \tag{14}$$

Now, define the $k^{th}$ *central moment* of a discrete random variable as follows:

$$\mathrm{E}[(\mathrm{X} - \mu)^k] = \sum_x (x - \mu)^k f_{\mathrm{X}}(x) \tag{15}$$

where μ, the *mean vector*, is given as the expectation of the individual elements of the vector:

$$\mu = \mathrm{E}[\mathrm{X}] = \mathrm{E}\begin{bmatrix}\mathrm{X}_1\\ \mathrm{X}_2\\ \vdots\\ \mathrm{X}_N\end{bmatrix} = \begin{pmatrix}\mathrm{E}[\mathrm{X}_1]\\ \mathrm{E}[\mathrm{X}_2]\\ \vdots\\ \mathrm{E}[\mathrm{X}_N]\end{pmatrix} \tag{16}$$

Finally, the *covariance matrix* **P** is given as the expectation of the product of two mean vectors, as follows [16]:

$$\mathbf{P} = \mathrm{E}[(\mathrm{X}-\mu)(\mathrm{X}-\mu)^{\mathrm{T}}] =$$

$$= \mathrm{E}\begin{bmatrix}(\mathrm{X}_1-\mu_1)^2 & (\mathrm{X}_1-\mu_1)(\mathrm{X}_2-\mu_2) & \cdots & \cdots & (\mathrm{X}_1-\mu_1)(\mathrm{X}_N-\mu_N)\\ (\mathrm{X}_2-\mu_2)(\mathrm{X}_1-\mu_1) & (\mathrm{X}_2-\mu_2)^2 & \vdots & \vdots & (\mathrm{X}_2-\mu_2)(\mathrm{X}_N-\mu_N)\\ \vdots & \vdots & (\mathrm{X}_3-\mu_3)^2 & \vdots & \vdots\\ \vdots & \vdots & \vdots & \ddots & \vdots\\ (\mathrm{X}_N-\mu_N)(\mathrm{X}_1-\mu_1) & (\mathrm{X}_N-\mu_N)(\mathrm{X}_2-\mu_2) & \cdots & \cdots & (\mathrm{X}_N-\mu_N)^2\end{bmatrix} \tag{17}$$

If there are *N* elements within the state-space, Equation 17 shows that the elements of the covariance matrix are product of every combination of elements, 1 through *N*. The expectation operator can be distributed to each element of the matrix, like is shown with the vector in Equation 16. Essentially, the covariance matrix provides the *weighted average* between all the elements of the vectors in a state-space. Thus, if the state-space is composed of position vectors, particularly of the particles in an ensemble cloud, the covariance matrix is measures the variability between the coordinates of every pair of elements within that ensemble cloud.

The trace of a square matrix is the sum of its diagonal elements. With an input of position vectors, the trace of the covariance matrix will compute the variance between each particle in the ensemble cloud. By defining this as the quantity of interest, the upper bound on the AMC simulations will define the distance a particle is "allowed" to vary from the cloud representation of the debris element.

With the aforementioned problem setup, system dynamics, and the now-defined QoI, the conjunction scenario of interest is ready to be analyzed with the AMC platform. The following data is presented at the

user-defined accuracy bound of 1e-3, bootstrap sampling size of 10,000 particles, and 3000-particle starting size for the ensemble.

## III. Results

The aim of this thesis is to identify a conjunction event in GEO and make a conclusion about probability of collision. The first step of this research process was a formal literature review concerning conjunction events and choosing a scenario for analysis. The AMC platform requires a complete picture of initial condition dynamics in order to propagate an ensemble cloud for an object. After obtaining this data, the simulations can be iterated and adjusted to determine collision risk.

Based on the required dynamics of the AMC platform, it was decided to keep the research focused on events in GEO to minimize perturbations. Candidates such as AMC-9 [17], Echostar, and Briz-M were considered, and the latter chosen due to the existence of robust initial condition data for position and velocity of the rocket body and a sample of its debris particles [11]. This data is shown below, in the form of two-line element sets (TLEs):

```
COSMOS 2513
1 41121U 15075A   22088.53590909 -.00000160  00000+0  00000+0 0  9993
2 41121   0.0487 111.4561 0001634 290.0303  58.5758  1.00271479 23071
BREEZE-M R/B
1 41122U 15075B   22088.16382857 -.00000112  00000+0  00000+0 0  9991
2 41122   4.9418  75.4544 0314038 115.1945 248.3298  1.04639835 24070
BREEZE-M DEB
1 41543U 15075D   22087.08677213 -.00000169  00000+0  00000+0 0  9993
2 41543   4.8981  75.9031 0251011 128.3259 234.1774  1.05309006 23843
BREEZE-M DEB
1 41544U 15075E   22085.75073562 -.00000093  00000+0  00000+0 0  9999
2 41544   4.8617  77.4035 0296942 127.7436 235.1900  1.05679617 23922
BREEZE-M DEB
1 41546U 15075G   22087.24562156 -.00000076  00000+0  00000+0 0  9990
2 41546   4.9117  79.2473 0237759 114.0105 248.7256  1.04637867 23697
BREEZE-M DEB
1 41547U 15075H   22087.99248154 -.00000274  00000+0  00000+0 0  9992
2 41547   4.9882  79.9733 0256260  88.8337 274.3370  1.03192339 23372
BREEZE-M DEB
1 41548U 15075J   22087.55273302 -.00000182  00000+0  00000+0 0  9996
2 41548   5.1910  69.3245 0363971  90.0088 274.3555  1.02195067 23516
```

***Figure 1:*** *TLE Data for Briz-M (2015-075B)*

The first TLE is for the Cosmos 2513 satellite, the second for the Briz-M rocket body, and third to seventh TLEs for select pieces of debris resulting from the explosion. Interpreting this data gives the following Keplerian orbital elements:

***Table 1:*** *Keplerian Orbital Elements for Briz-M (2015-075B)*

| | **Semimajor Axis** [km] | **Eccentricity** | **Inclination** [deg] | **Longitude of the Ascending Node** [deg] | **Argument of Periapsis** [deg] | **True Anomaly** [deg] |
|---|---|---|---|---|---|---|
| **Cosmos 2513** | 42165.1 | 0.000344 | 0.0493 | 1.942454 | 112.4326 | 186.6793 |
| **Briz-M R/B** | 40982.6 | 0.031529 | 4.5582 | 1.344848 | 109.9295 | 253.6303 |
| **Debris 1** | 40809.0 | 0.025254 | 4.5183 | 1.353616 | 123.0286 | 239.5613 |
| **Debris 2** | 40713.7 | 0.029686 | 4.4833 | 1.381976 | 122.4636 | 240.5887 |
| **Debris 3** | 40983.4 | 0.023936 | 4.5113 | 1.417246 | 108.4608 | 254.4321 |
| **Debris 4** | 41365.5 | 0.025800 | 4.5886 | 1.428981 | 83.4475 | 279.6369 |
| **Debris 5** | 41634.7 | 0.036930 | 4.8152 | 1.227874 | 85.8775 | 278.4338 |

This data can then be translated to Cartesian or equinoctial coordinates; the former is useful for initial orbit visualization, and the latter a necessity for use in the AMC platform.

Translation into Cartesian coordinates provides classical position and velocity values (see Equation 5) at initial time $t_0$. These values can be used to propagate the expected orbits for each object, shown in the following figure.

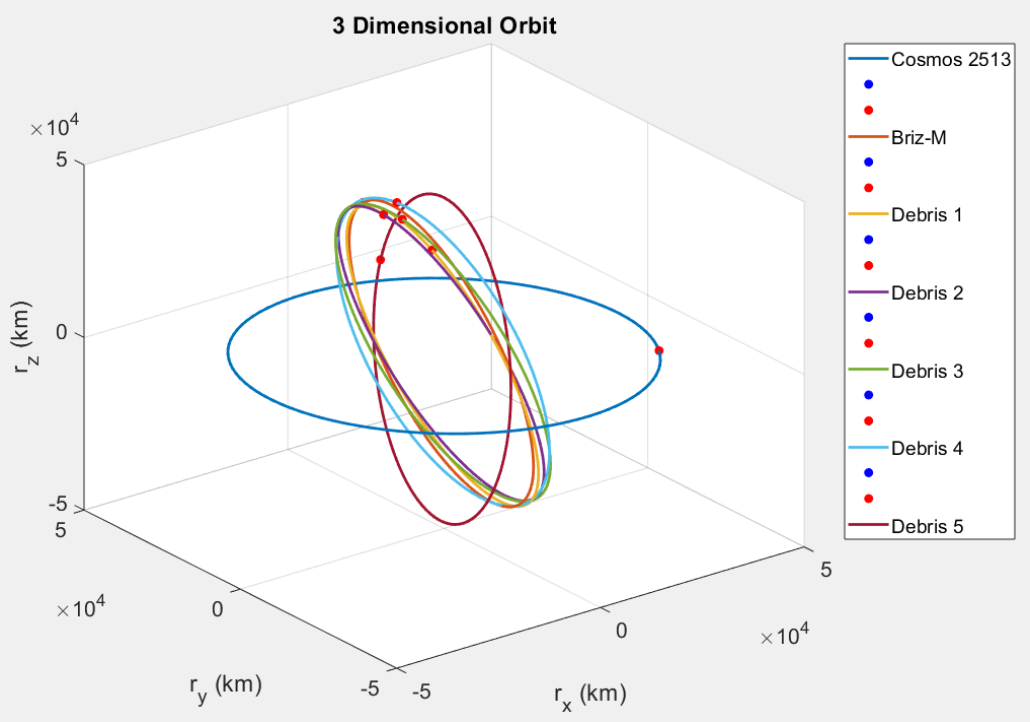


***Figure 2:*** *Orbit Visualizations for Briz-M (2015-075B)*

The horizontal orbit is the Cosmos 2513 satellite, effectively injected into GEO, and the rest of the orbits are the Briz-M rocket stage and the five debris objects. The red and blue dots mark the starting and ending positions of the RSOs. Since these objects are in GEO, perturbations are minimal, thus these objects are expected to remain in the orbits visualized above for many years.

The next step was to perform a preliminary conjunction analysis to determine which objects, if any, experience a close approach between each other. Initially, the difference of the position vectors was taken at each point between two orbits at the same timestep (modeled over 10,000 points). This did not produce any interesting results, i.e., a worthwhile close approach. Thus, the initial conditions were adjusted so that a given point in the orbit of object A was compared to *every* point in the orbit of object B to find the closest approach. Using this technique, the closest approach for every pairing is provided in the following table:

***Table 2:*** *Close Approaches for Briz-M (2015-075B)*

| Object Pairing | Close Approach (km) | Object Pairing | Close Approach (km) |
|---|---|---|---|
| **1 and 2** | 122.264 | **2 and 6** | 158.236 |
| **1 and 3** | 432.529 | **3 and 6** | 72.974 |
| **2 and 3** | 89.883 | **4 and 6** | 109.646 |
| **1 and 4** | 233.487 | **5 and 6** | 240.543 |
| **2 and 4** | 172.485 | **1 and 7** | 244.043 |
| **3 and 4** | 7.460 | **2 and 7** | 552.164 |
| **1 and 5** | 1141.055 | **3 and 7** | 610.550 |
| **2 and 5** | 1424.739 | **4 and 7** | 719.050 |
| **3 and 5** | 1310.165 | **5 and 7** | 1146.335 |
| **4 and 5** | 211.797 | **6 and 7** | 1704.257 |
| **1 and 6** | 630.635 | Note: Object 1 represents the Echostar satellite, and Object 2 represents the Briz-M body | |

As noted in the table, object 1 represents the Echostar satellite, object 2 is the Briz-M rocket body, and objects 3-7 signify the five pieces of debris. While most close approaches are on the order of a few hundred kilometers, object 3 and object 4, aka “Debris 1” and “Debris 2”, are the only pairing with an approach of less than ten kilometers. Thus, this orbital debris pairing was chosen as the conjunction of interest, to be further analyzed via the AMC platform.

A preliminary analysis was performed on the object pairing to determine the starting point for the AMC simulations. Using the timestamp that resulted in the close approach determined earlier as the starting point, orbits were propagated for the two pieces of debris. This is visualized in the plot on the left in Figure 3, with those starting points marked on the graph. At this initial timestamp, object 3 appears to be at the hypothetical point of conjunction, i.e., where the two orbits cross paths, but object 4 is slightly ahead in its orbital path. Thus, the time vector for object 4 was manually adjusted, shown in the middle plot, until it appeared to overlap the conjunction zone.

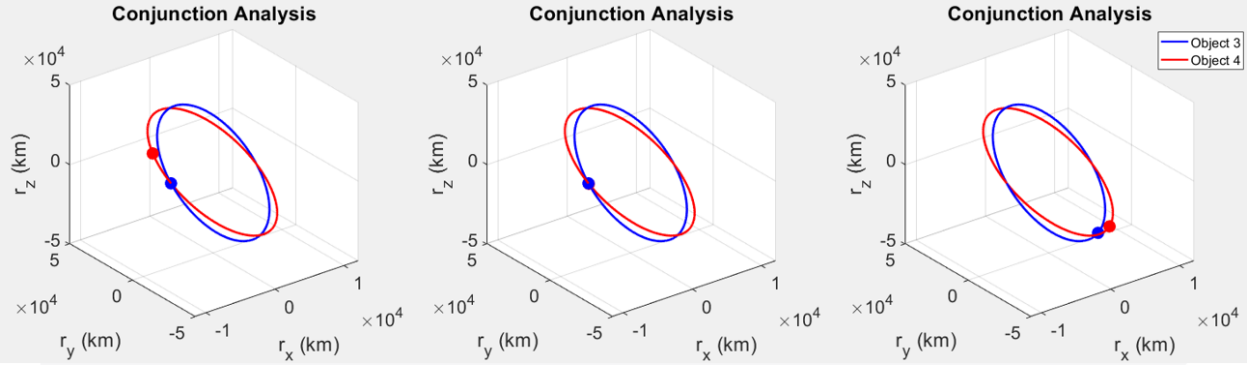


***Figure 3:*** *Preliminary Conjunction Analysis for Object 3 (blue) and Object 4 (red)*

With the conjunction timestamps now defined, both orbits were "backed up" 7.2 hours, or one-third of the time for one complete orbit, so that the close-approach itself would happen in the middle of the simulations at a predictable time. This is visualized in the plot on the right of Figure 3.

The simulations were performed for three days of orbital motion, with the AMC platform producing ensemble clouds at 11 points throughout the propagation. Figure 4 shows the growth of the ensemble clouds at timestamps 2, 5, 8, and 11.

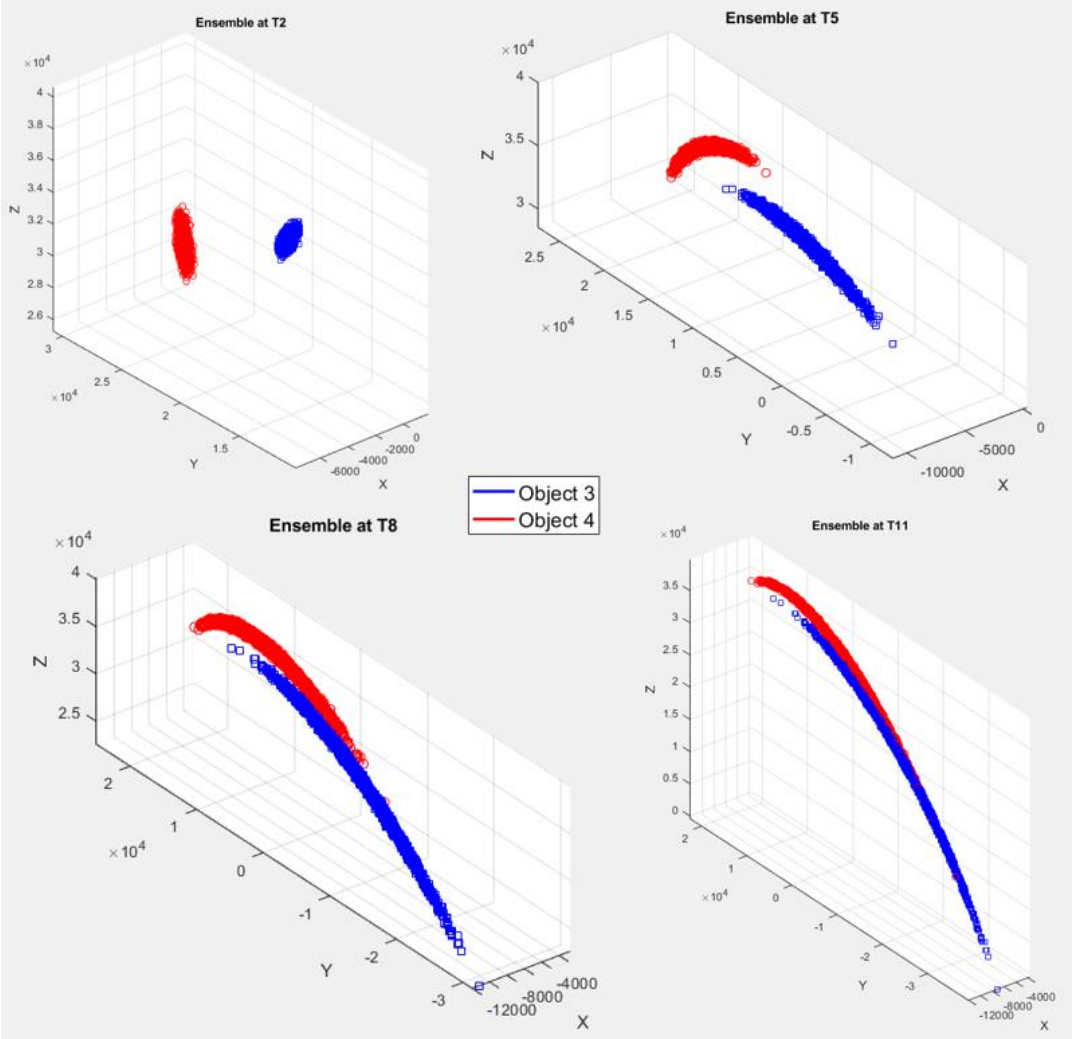


***Figure 4:*** *Growth of Ensemble Clouds for Object 3 (blue) and Object 4 (red)*

After obtaining the ensemble results, probability of collision can be computed by discretizing the domain of conjunction into a grid and determining there are particles for both objects' ensembles present within that convex hull volume. A numerical value is gained using this ratio:

$$P_c = \frac{\sum_{i=1}^{N} \min\,(m_i, n_i)}{\sum_{j=1}^{N} \max\,(m_j, n_j)} \tag{18}$$

where $m_i$, $n_i$, $m_j$, and $n_j$ correspond to the number of particles within the grid partition for each ensemble at a certain timestamp. Using this definition, the probability of collision between objects 3 and 4 remained

zero until the final timestamp, T11. To understand why this is the case, Figure 5 shows the growth of the ensemble clouds at particular timestamps along the orbits.

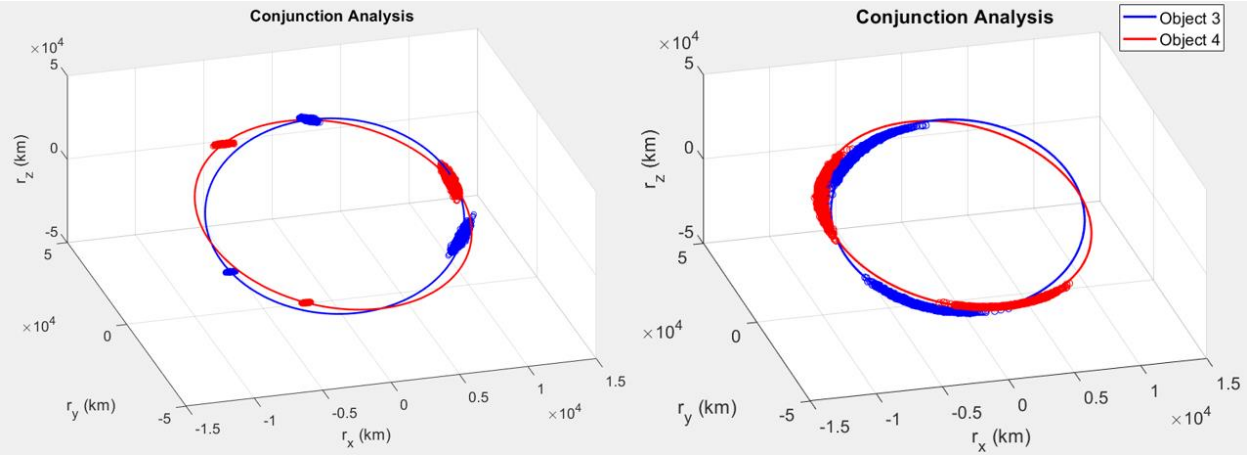


***Figure 5:*** *Ensemble Cloud Visualizations: T1, T2, T3 (left) and T7, T8 (right)*

As can be seen in these plots, as the two ensemble clouds grow, they get closer to overlapping with each other and the point of close approach. However, it isn't until T11 (Figure 6) that particles representing objects 3 and 4 significantly intersect.

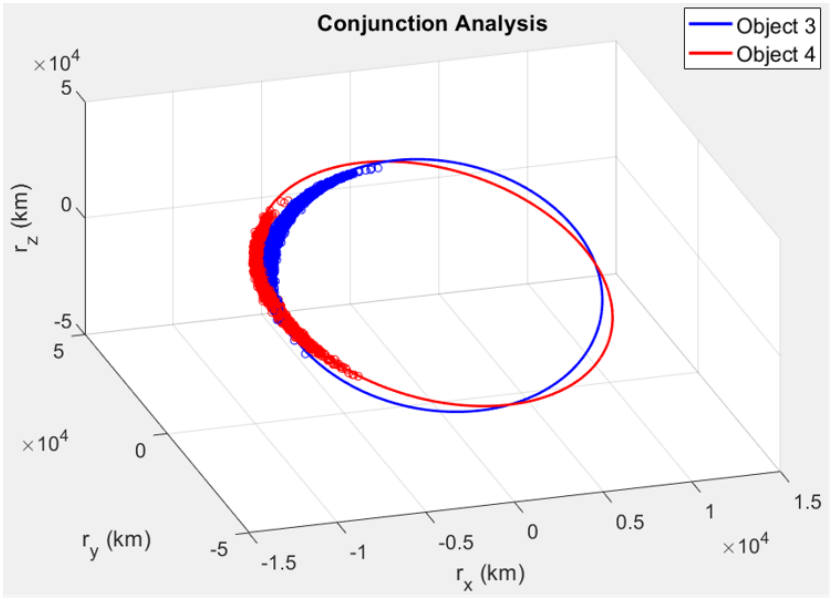


***Figure 6:*** *Ensemble Cloud Visualization: T11*

When it comes to a numerical value for probability of collision, it depends largely on the grid size (*N*) for the convex hull volume. For the same two ensemble clouds at the same timestamp, the bounds of the volume remain the same; what changes is the number of smaller portions the volume is divided into. A lower grid size will result in a higher probability of collision because the likelihood that particles from both ensembles will be present in the same portion of the grid increases as the size of the subdivisions grows. Probability of collision for various grid sizes was calculated, tabulated below.

***Table 3:*** *Probability of Collision for Various Grid Sizes*

| Grid Size (N) | Probability of Collision |
|---|---|
| **15** | 0.04639 |
| **25** | 0.02951 |
| **50** | 0.01317 |
| **100** | 0.00976 |
| **200** | 0.00418 |

According to literature, a value on the scale of $10^{-4}$ is deemed significant enough to warrant a maneuver to avoid a collision. Thus, this result is in the threshold for a conjunction risk.

## IV. Conclusion

The adaptive Monte Carlo platform is a robust and highly reliable tool for uncertainty forecasting within defined accuracy bounds. With a complete set of initial condition data, predictive analysis can be performed on an object in geostationary orbit with a guaranteed level of accuracy. The dynamics of the RSOs resulting from the 2016 Briz-M explosion showed that probability of collision between the rocket body and its largest pieces of debris is significant. Specifically, the analysis was performed on the two objects that were determined to have the highest collision risk through preliminary investigation of their dynamics via orbital propagation. For those pieces of debris, at a convex hull volume grid size of 100, probability of collision was found to be close to 0.01. If a satellite or rocket was approaching an object at

a risk this high, a relocation maneuver would be warranted. Further work can be done to analyze this object pairing by making adjustments to the propagation time and ensemble timestamps in the AMC platform. The Briz event can be further explored by performing the same level of conjunction analysis on all object pairings to get a more complete picture of the scenario. Additionally, all user-defined conditions, including required level of accuracy and starting ensemble size, can be refined to increase the reliability of the results. Another way to deepen this investigation is to compare the AMC results to a non-adaptive version of the Monte Carlo platform, or another uncertainty forecasting platform altogether, to get a better sense of AMC's reliability. Lastly, an additional problem worth exploring could be to perform a reverse-propagation on the two objects to see if AMC would predict they collide, as a way of verifying the platform with a known end result. In general, it is important to take this work in a broader context; while predictive analysis is important and useful for preventing conjunction events, it is the responsibility of aerospace companies, research scientists, and engineers to implement these strategies and be cognizant of what they send up into orbit.

## Appendix A

Probability of Collision Code

```
function Pc = Prob_Collision_grid(obj1, obj2)

h = figure(3);
plot3(obj1(:, 1), obj1(:, 2), obj1(:, 3), 'ro');
hold on;
plot3(obj2(:, 1), obj2(:, 2), obj2(:, 3), 'bs');
hold on;
axis equal;
xlabel('X');
ylabel('Y');
% savefig(h, ['figs/conjunction_', num2str(floor(time)), '.fig'], 'compact')
% close(h);
%minimums and maximums for of each object to determine where the grid needs to be
min_obj1 = min(obj1);
min_obj2 = min(obj2);
max_obj1 = max(obj1);
max_obj2 = max(obj2);

min_both = min([min_obj1; min_obj2]);
max_both = max([max_obj1; max_obj2]);

%break up the domain into 500 boxes in each dimension

%the conjunction generally happens in the vertical plane
x_vect = linspace(min_both(1), max_both(1), 100);
y_vect = linspace(min_both(2), max_both(2), 100);
z_vect = linspace(min_both(3), max_both(3), 100);
edge_x = abs(x_vect(2) - x_vect(1));
edge_y = abs(y_vect(2) - y_vect(1));
edge_z = abs(z_vect(2) - z_vect(1));

%generate the convex hull for the
%check if a point is in the generated cube. If it is, remove it from the
%list to avoid checking it again in an adjacent cube
data_obj1 = obj1;
data_obj2 = obj2;
pts_in_obj1 = zeros(length(x_vect), length(y_vect), length(z_vect));
pts_in_obj2 = zeros(length(x_vect), length(y_vect), length(z_vect));
num = 0;
den = 0;
for i = 1:length(x_vect)
    Dom(1,1) = x_vect(i);
    Dom(1,2) = Dom(1,1) + edge_x;
    for j = 1:length(y_vect)
        Dom(2,1) = y_vect(j);
        Dom(2,2) = Dom(2,1) + edge_y;
        for k = 1:length(z_vect)
%             origin = [x_vect(i) y_vect(j) z_vect(k)];
%             cube = cell2mat(arrayfun(@(x,y,z) x*y+z, XYZ, ...
%                 repmat(edges,size(XYZ,1),1), repmat(origin,size(XYZ,1),1),
'UniformOutput', false));
%             c_ref = convhulln(cube);
            Dom(3,1) = z_vect(k);
            Dom(3,2) = Dom(3,1) + edge_z;
            %for this specific grid cube, what points of ensemble 1 are within it
            check_obj1 = zeros(1,size(data_obj1,1));
            check_obj2 = zeros(1,size(data_obj2,1));
```

```
            lsize      = max([length(check_obj1), length(check_obj2)]);
            %for m = 1:size(data_obj1,1)
            in = zeros(size(data_obj1,1),3);
            in2 = zeros(size(data_obj2,1),3);
            in(:,1) = data_obj1(:,1) >= Dom(1,1) & data_obj1(:,1)<=Dom(1,2);
            in(:,2) = data_obj1(:,2) >= Dom(2,1) & data_obj1(:,2)<=Dom(2,2);
            in(:,3) = data_obj1(:,3) >= Dom(3,1) & data_obj1(:,3)<=Dom(3,2);
            check_obj1 = all(in,2);
            in2(:,1) = data_obj2(:,1) >= Dom(1,1) & data_obj2(:,1)<=Dom(1,2);
            in2(:,2) = data_obj2(:,2) >= Dom(2,1) & data_obj2(:,2)<=Dom(2,2);
            in2(:,3) = data_obj2(:,3) >= Dom(3,1) & data_obj2(:,3)<=Dom(3,2);
            check_obj2 = all(in2,2);
%             for m = 1:lsize
%                 if m <= length(check_obj1)
% %                     cube_obj1     = [cube;data_obj1(m,:)];
% %                     c_obj1        = convhulln(cube_obj1);
% %                     check_obj1(m) = all(ismember(c_ref, c_obj1, 'rows'));
%                     check_obj1(m) = inDomain(Dom,data_obj1(m,:));
%                 end
%                 if m <= length(check_obj2)
% %                     cube_obj2     = [cube;data_obj2(m,:)];
% %                     c_obj2        = convhulln(cube_obj2);
% %                     check_obj2(m) = all(ismember(c_ref, c_obj2, 'rows'));
%                    check_obj2(m) = inDomain(Dom,data_obj2(m,:));
%                 end
%             end
            %number of pts within the specific grid for object 1
            pts_in_obj1(i,j,k) = sum(check_obj1);
            %remove the data as its already known and been checked
            if any(check_obj1)
                data_obj1(find(check_obj1), :, :) = [];
            end

%             %for this specific grid cube, what points of ensemble 1 are within it
%             check_obj2 = zeros(1,size(data_obj2,1));
%             for m = 1:size(data_obj2,1)
%                 cube_obj2     = [cube;data_obj2(m,:)];
%                 c_obj2        = convhulln(cube_obj2);
%                 check_obj2(m) = all(ismember(c_ref, c_obj2, 'rows'));
%             end

            %number of pts within the specific grid for object 1
            pts_in_obj2(i,j,k) = sum(check_obj2);
            %remove the data as its already known and been checked
            if any(check_obj2)
                data_obj2(find(check_obj2), :, :) = [];
            end

            num = num + min(pts_in_obj1(i,j,k), pts_in_obj2(i,j,k));
            den = den + max(pts_in_obj1(i,j,k), pts_in_obj2(i,j,k));

            if isempty(data_obj2) && isempty(data_obj1)
                break;
            end
        end
    end
end
Pc = num / den;

end
```

**Appendix B**

Monte Carlo Equations

$$\bar{h}(\mathbf{x}_t) \triangleq E_{\mathcal{W}_t}[h(\mathbf{x}_t)] = \int_{\Omega_t} h(\mathbf{x}_t)\mathcal{W}_t d\mathbf{x}_t \tag{1}$$

$$d\mathbf{x} = \mathbf{f}(t,\mathbf{x})dt \ \ , \ \ \mathbf{x}_0 \sim \mathcal{W}_0(t_0,\mathbf{x}) \tag{2}$$

$$\frac{\partial}{\partial t}\mathcal{W}(t,\mathbf{x}) = \mathcal{L}[\mathcal{W}(t,\mathbf{x})] = -\sum_{i=1}^{N}\left(f_i\frac{\partial \mathcal{W}}{\partial x_i} + \mathcal{W}\frac{\partial f_i}{\partial x_i}\right) \tag{3}$$

$$\mathbf{r} = -\frac{\mu_\oplus}{\|\mathbf{r}\|^3}\mathbf{r} + \mathbf{F}(\mathbf{r}) \tag{4}$$

$$\mathbf{x}_{CE} = \begin{bmatrix} x \\ y \\ z \\ v_x \\ v_y \\ v_z \end{bmatrix}, \ \mathbf{x}_{OE} = \begin{bmatrix} a\text{: semi} - \text{major axis} \\ e\text{: eccentricity} \\ i\text{: inclination} \\ \Omega\text{: ascending node} \\ \omega\text{: argument of perigee} \\ M\text{: mean anomaly} \end{bmatrix}, \ \mathbf{x}_{EE} = \begin{bmatrix} a \\ P_1 = e\sin\varpi \\ P_2 = e\cos\varpi \\ Q_1 = \tan\frac{1}{2}i\sin\Omega \\ Q_2 = \tan\frac{1}{2}i\cos\Omega \\ l = \varpi + M \end{bmatrix} \tag{5}$$

$$\frac{da}{dt} = \frac{2a^2}{h}\left[(P_2\sin L - P_1\cos L)a_{dr} + \frac{p}{r}a_{d\theta}\right] \tag{6a}$$

$$\frac{dP_1}{dt} = \frac{r}{h}\{-\frac{p}{r}\cos L a_{dr} + \left[P_1 + \left(1+\frac{p}{r}\right)\sin L\right]a_{d\theta} - P_2(Q_1\cos L - Q_2\sin L)a_{dh}\} \tag{6b}$$

$$\frac{dP_2}{dt} = \frac{r}{h}\{\frac{p}{r}\sin L a_{dr} + \left[P_2 + \left(1+\frac{p}{r}\right)\cos L\right]a_{d\theta} + P_1(Q_1\cos L - Q_2\sin L)a_{dh}\} \tag{6c}$$

$$\frac{dQ_1}{dt} = \frac{r}{2h}(1+Q_1^2+Q_2^2)\sin L a_{dh} \tag{6d}$$

$$\frac{dQ_2}{dt} = \frac{r}{2h}(1+Q_1^2+Q_2^2)\cos L a_{dh} \tag{6e}$$

$$\frac{dl}{dt} = n - \frac{r}{h}\left\{\begin{matrix}\left[\frac{a}{a+b}\left(\frac{p}{r}\right)(P_1\sin L + P_2\cos L) + \frac{2b}{a}\right]a_{dr} \\ +\frac{a}{a+b}\left(1+\frac{p}{r}\right)(P_1\cos L - P_2\sin L)a_{d\theta} + (Q_1\cos L - Q_2\sin L)a_{dh}\end{matrix}\right\} \tag{6f}$$

$$l = K + P_1\cos K - P_2\sin K \tag{7}$$

$$r = a(1 - P_1\sin K - P_2\cos K). \tag{8}$$

$$\sin L = \frac{a}{r}\left[\left(1 - \frac{a}{a+b}P_2^2\right)\sin K + \frac{a}{a+b}P_1P_2\cos K - P_1\right] \tag{9a}$$

$$\cos L = \frac{a}{r}\left[\left(1 - \frac{a}{a+b}P_1^2\right)\cos K + \frac{a}{a+b}P_1P_2\sin K - P_2\right] \tag{9b}$$

$$\frac{a}{a+b} = \frac{1}{1+\sqrt{1-P_1^2-P_2^2}} \ . \tag{10}$$

$$\mathbf{a}_d = \frac{\mu_\oplus}{r^2}\sum_{k=2}^{4} J_{k,E}\left(\frac{r_E}{r}\right)^k [P'_{k+1}\mathbf{i}_{SO} - P'_k\mathbf{i}_z] \tag{11}$$

$$|\varepsilon_n| = \left|\bar{h} - \tilde{h}_n\right| \tag{12}$$

$$|\varepsilon_n| = \left|\bar{h} - \tilde{h}_n\right| \leq \mathcal{D}(\{x_0^i\}_{i=1}^n) V(S_t) \tag{13}$$

$$\mathrm{E}[g(\mathrm{X})] = \sum_x g(x) f_{\mathrm{X}}(x) \tag{14}$$

$$\mathrm{E}[(\mathrm{X} - \mu)^k] = \sum_x (x - \mu)^k f_{\mathrm{X}}(x) \tag{15}$$

$$\mu = \mathrm{E}[\mathrm{X}] = \mathrm{E}\begin{bmatrix} \mathrm{X}_1 \\ \mathrm{X}_2 \\ \vdots \\ \mathrm{X}_N \end{bmatrix} = \begin{pmatrix} \mathrm{E}[\mathrm{X}_1] \\ \mathrm{E}[\mathrm{X}_2] \\ \vdots \\ \mathrm{E}[\mathrm{X}_N] \end{pmatrix} \tag{16}$$

$$\mathbf{P} = \mathrm{E}[(\mathrm{X} - \mu)(\mathrm{X} - \mu)^{\mathrm{T}}] =$$

$$= \mathrm{E}\begin{bmatrix} (\mathrm{X}_1 - \mu_1)^2 & (\mathrm{X}_1 - \mu_1)(\mathrm{X}_2 - \mu_2) & \cdots & \cdots & (\mathrm{X}_1 - \mu_1)(\mathrm{X}_N - \mu_N) \\ (\mathrm{X}_2 - \mu_2)(\mathrm{X}_1 - \mu_1) & (\mathrm{X}_2 - \mu_2)^2 & \vdots & \vdots & (\mathrm{X}_2 - \mu_2)(\mathrm{X}_N - \mu_N) \\ \vdots & \vdots & (\mathrm{X}_3 - \mu_3)^2 & \vdots & \vdots \\ \vdots & \vdots & \vdots & \ddots & \\ (\mathrm{X}_N - \mu_N)(\mathrm{X}_1 - \mu_1) & (\mathrm{X}_N - \mu_N)(\mathrm{X}_2 - \mu_2) & \cdots & \cdots & (\mathrm{X}_N - \mu_N)^2 \end{bmatrix} \tag{17}$$

$$P_c = \frac{\sum_{i=1}^{N} \min(m_i, n_i)}{\sum_{j=1}^{N} \max(m_j, n_j)} \tag{18}$$

**References**


[1] Anandhi, Chandran, Hemasai, Mani, and Kumar. “Statistical Studies on Space Launches and the Need for Active Debris Removal System.” AIAA SPACE Forum, 2015.

[2] https://astronomy.com/news/2021/09/how-many-satellites-are-orbiting-earth

[3] National Aeronautics and Space Administration, “Satellite Collision Leaves Significant Debris Clouds,” Orbital Debris Quarterly News, vol. 13, no. 2, Apr-2009.

[4] https://www.cnn.com/2021/12/03/world/iss-space-debris-russia-intl/index.html

[5] https://www.nasa.gov/mission_pages/station/news/orbital_debris.html

[6] VanFossen, A., Mangel, A., Kumar, M., “Efficacy of Parallelization in Adaptive Monte Carlo for Forecasting in GEO”, AIAA Sci-Tech Forum, 2022, 3-7 January.

[7] Yang, C., and Kumar, M., “Discrepancy Driven Adaptive Monte Carlo for Forward Uncertainty Forecasting in Nonlinear Dynamical Systems,” 2018 Annual American Control Conference (ACC), 2018.

[8] Yang, C., and Kumar, M., “Closed-Loop Adaptive Monte Carlo Framework for Uncertainty Forecasting in Nonlinear Dynamic Systems.” Journal of Guidance, Control, and Navigation, June 2019.

[9] National Aeronautics and Space Administration, “*Briz-M* Core Stage Fragments Near GEO Orbit,” Orbital Debris Quarterly News, vol. 20, Apr-2016.

[10] Agapov, V., Zelenov, D., Lapshin, A., Khutorovsky, Z., “Expanding Knowledge on Real Situation at High Near-Earth Orbits,” Proc. 7th European Conference on Space Debris, Darmstadt, Germany, 18–21 April 2017.

[11] https://celestrak.com/NORAD/elements/gp.php?INTDES=2015-075

[12] Øksendal, B., Stochastic Differential Equations: An Introduction with Applications, 6th ed., Universitext, Springer-Verlag Berlin Heidelberg, 2003.

[13] Gazzino, C., “Dynamics of a Geostationary Satellite,” Research Report Rapport LAAS n° 17432, LAAS-CNRS, Nov. 2017.

[14] Battin, R. H., An Introduction to the Mathematics and Methods of Astrodynamics, Revised Edition, American Institute of Aeronautics and Astronautics, 1999.

[15] VanFossen, A., Kumar, M., “Determination of Efficient Quantities of Interest for Space Situational Awareness and Adaptive Monte Carlo,” AAS 21-276.

[16] Kumar, M., “AAE 8194: Random Dynamic Systems,” Random Variables: Part II.

[17] https://www.agi.com/missions/space-operations-missions/amc-9-neighborhood-watch